

Sea quark and gluon polarization in the nucleon at NLO accuracy.*

D. de Florian,^{1,†} G. A. Navarro,^{1,‡} and R. Sassot^{1,§}

¹*Departamento de Física, Universidad de Buenos Aires
Ciudad Universitaria, Pab.1 (1428) Buenos Aires, Argentina*

(Dated: July 7, 2018)

We investigate the sea quark polarization in the nucleon by means of a combined next to leading order analysis to the recently enlarged set of inclusive and semi-inclusive polarized deep inelastic scattering data. Using the Lagrange multiplier method, we assess the uncertainty inherent to the extraction of the different spin dependent parton densities in a QCD global fit, and the impact of the increased set of semi-inclusive data now available. We comment on future prospects at RHIC and JLAB and their potential impact in the future determination of polarized parton densities.

PACS numbers: 12.38.Bx, 13.85.Ni

Keywords: Semi-Inclusive DIS; perturbative QCD.

I. INTRODUCTION

For more than fifteen years, polarized inclusive deep inelastic scattering (pDIS) has been the main, if not unique, source of information on how the individual partons in the nucleon are polarized at very short distances. Hadronic decays, of course, bring us from lower energies hints about the relations between the net polarization of each flavor, but only after making strong assumptions about flavor symmetry within the nucleon. These kind of assumptions, however, have been seriously challenged by data over the last decade, at least in the realm unpolarized experiments [1, 2].

The electromagnetic nature of the dominant interaction between the leptonic probe and the target in the pDIS experiments performed so far, does not allow to disentangle quark from anti-quark contributions, and thus valence quark from sea quarks. Consequently, in spite of strenuous efforts and very successful experimental programs run by several collaborations, our knowledge of the detailed spin dependent parton distribution functions (pPDF) has been held hostage to a large extent by our own assumptions. Most notably, the sea quark densities and also that for the gluons. The latter, because it influences the pDIS observables mainly through their energy scale dependence. Although at next to leading order accuracy the gluon density contributes to the pDIS cross section directly, this contribution is relatively suppressed.

Many alternative experiments have been conceived, and in some cases already implemented, to improve this situation. The most mature among them are those based on polarized semi-inclusive deep inelastic scattering (pSIDIS), i.e. a pDIS experiment where a particular hadron is tagged in the hadronic final state. Choosing different target and final state hadrons, the respective cross sections are sensitive to different combinations of flavored quarks and anti-quarks, to be disentangled. These experiments began with the pioneering efforts of SMC, in the late nineties [3], followed by those of HERMES at DESY [4], and lately COMPASS at CERN [5], and are planned to be improved at the Thomas Jefferson National Laboratory (JLAB) in the near future [6].

The phenomenological impact of the pSIDIS data proved to be encouraging although scarce in the initial stage: the reduced number of data and the relatively large estimated errors, at best allowed to check the consistency between pDIS and pSIDIS in a variety of spin-flavor symmetry scenarios [7, 8, 9]. With the availability of larger sets of pSIDIS data, much more precise, and for final state hadrons and targets of different flavor composition, the situation now has changed dramatically. pSIDIS data have a non negligible weight in combined global fits at present, comparable to that of inclusive data, and also show clear preferences for the light sea quark polarization. It also helps to constrain the strange sea quark and gluon polarization complementing the information already obtained from pDIS.

Although we can now leave behind the spin-flavor symmetry assumption, translating polarized observables to parton distributions always imply the use of some additional piece of information. In the case of pDIS, we need the unpolarized structure function F_1 , or a set of unpolarized parton densities (PDFs), in order to go from the pPDFs

*Partially supported by CONICET, Fundación Antorchas, UBACYT and ANPCyT, Argentina.

[†]Electronic address: deflo@df.uba.ar

[‡]Electronic address: gabin@df.uba.ar

[§]Electronic address: sassot@df.uba.ar

to the measured asymmetries. For pSIDIS we also need a set of fragmentation functions (FFs), the functions that measure the probability of a quark fragmenting into a given hadron [10, 11], and polarized fracture functions [13] if target fragmentation events are taken into account, or a Monte Carlo generator modeling these same processes. The results of the global analyses to polarized data show negligible differences when using different sets of modern PDFs [2, 12], but the differences are sizable when using different FFs, a feature to be taken into account when assessing the uncertainties of the pPDFs. Eventually, pSIDIS data will help to constrain FFs, including it along with electron-positron annihilation data in the global fits where they come from.

In the following we perform a combined next to leading order analysis to the recently updated set of pDIS and pSIDIS data, and present the resulting pPDFs. Specifically, we focus on the extraction of sea quark and gluon densities, analyzing the constraining power of either set of data on the individual densities. As result, we find not only a complete agreement between pDIS and pSIDIS data, but a very useful complementarity, leading to rather well constrained densities.

Using the Lagrange multiplier approach [30], we explore the profile of the χ^2 function against different degrees of polarization in each parton flavor. In this way we obtain estimates for the uncertainty in the net polarization of each flavor, and in the parameters of the pPDFs. We compare results obtained with the two most recent sets of fragmentation functions, and also within the leading (LO) and next to leading order (NLO) approximation. The differences found using alternative sets of FF are found to be within conservative estimates for the uncertainties. Nevertheless, there is a clear preference for a given set of FF over the other, shown in a difference of several units in the χ^2 of the respective global fits. In NLO global fits the overall agreement between theory and the full set of data is sensibly higher than in LO case.

Finally, we analyze the behavior of the cross section for longitudinally polarized proton-proton collisions into neutral pions with a wide range of pPDFs sets coming from a rather conservative uncertainty interval. This observable is found to be crucially sensitive to the polarized gluon density and therefore an invaluable tool. We compute the required precision to be reached in the programed experiments in order to constrain even further this distribution and also future sets of pPDFs. A similar analysis is made for forthcoming pSIDIS data to be obtained at JLAB.

II. CONVENTIONS AND DATA SETS

Throughout the present analysis, we follow the same conventions and definitions for the polarized inclusive asymmetries and parton densities adopted in references [7, 8, 9], however we use more recent inputs, such as unpolarized parton densities [12] and the respective values for α_s . In the totally inclusive case, the spin dependent asymmetries are given by [14]

$$A_1^N(x, Q^2) = \frac{g_1^N(x, Q^2)}{F_1^N(x, Q^2)} = \frac{g_1^N(x, Q^2)}{F_2^N(x, Q^2)/2x[1 + R^N(x, Q^2)]}, \quad (1)$$

where the inclusive spin-dependent nucleon structure function $g_1^N(x, Q^2)$ can be written at NLO as a convolution between polarized parton densities for quarks and gluons, $\Delta q_i(x, Q^2)$ and $\Delta g(x, Q^2)$, respectively, and coefficient functions $\Delta C_i(x)$ [15]

$$g_1^N(x, Q^2) = \frac{1}{2} \sum_{q, \bar{q}} e_q^2 \left[\Delta q(x, Q^2) + \frac{\alpha_s(Q^2)}{2\pi} \int_x^1 \frac{dz}{z} \left\{ \Delta C_q(z) \Delta q\left(\frac{x}{z}, Q^2\right) + \Delta C_g(z) \Delta g\left(\frac{x}{z}, Q^2\right) \right\} \right]. \quad (2)$$

A more detailed discussion about these coefficient functions and their factorization scheme dependence can be found in Ref.[16]. $F_1^N(x, Q^2)$ is the unpolarized nucleon structure function that can be written in terms of $F_2^N(x, Q^2)$ and R , the ratio of the longitudinal to transverse cross section [14]. The use of the QCD NLO approximations both in $F_1^N(x, Q^2)$ and in $g_1^N(x, Q^2)$ has been shown to reduce the sensitivity of PDFs to higher twists [17].

Analogously, for the semi-inclusive asymmetries we have:

$$A_1^{Nh}(x, Q^2) |_Z \simeq \frac{\int_Z dz g_1^{Nh}(x, z, Q^2)}{\int_Z dz F_1^{Nh}(x, z, Q^2)}, \quad (3)$$

where the superscript h denotes the hadron detected in the final state, and the variable z is given by the ratio between the hadron energy and that of the spectators in the target. The region Z , over which z is integrated, is determined by kinematical cuts applied when measuring the asymmetries.

For the spin dependent structure function $g_1^N(x, Q^2)$, we use the NLO expression [18]

$$g_1^{N^h}(x, z, Q) = \frac{1}{2} \sum_{q, \bar{q}} e_q^2 \left[\Delta q(x, Q^2) D_q^H(z, Q^2) + \frac{\alpha_s(Q^2)}{2\pi} \int_x^1 \frac{d\hat{x}}{\hat{x}} \int_z^1 \frac{d\hat{z}}{\hat{z}} \left\{ \Delta q\left(\frac{x}{\hat{x}}, Q^2\right) \Delta C_{q\bar{q}}^{(1)}(\hat{x}, \hat{z}, Q^2) D_q^H\left(\frac{z}{\hat{z}}, Q^2\right) \right. \right. \\ \left. \left. + \Delta q\left(\frac{x}{\hat{x}}, Q^2\right) \Delta C_{gq}^{(1)}(\hat{x}, \hat{z}, Q^2) D_g^H\left(\frac{z}{\hat{z}}, Q^2\right) + \Delta g\left(\frac{x}{\hat{x}}, Q^2\right) \Delta C_{q\bar{q}}^{(1)}(\hat{x}, \hat{z}, Q^2) D_q^H\left(\frac{z}{\hat{z}}, Q^2\right) \right\} \right], \quad (4)$$

and in order to avoid the convolution integrals in \hat{x} and \hat{z} we switch to moment space in both variables as suggested in [19] and already implemented in [9].

For u and d quarks *plus* anti-quarks densities at the initial scale $Q_0^2 = 0.5 \text{ GeV}^2$ we propose

$$x(\Delta q + \Delta \bar{q}) = N_q \frac{x^{\alpha_q} (1-x)^{\beta_q} (1 + \gamma_q x^{\delta_q})}{B(\alpha_q + 1, \beta_q + 1) + \gamma_q B(\alpha_q + \delta_q + 1, \beta_q + 1)} \quad q = u, d \quad (5)$$

where $B(\alpha, \beta)$ is the standard beta function, while for strange quarks *plus* anti-quarks we use

$$x(\Delta s + \Delta \bar{s}) = 2N_s \frac{x^{\alpha_s} (1-x)^{\beta_s}}{B(\alpha_s + 1, \beta_s + 1)}, \quad (6)$$

with a similar parametric form for gluons

$$x\Delta g = N_g \frac{x^{\alpha_g} (1-x)^{\beta_g}}{B(\alpha_g + 1, \beta_g + 1)}. \quad (7)$$

The first moments of the quark densities δq (N_q)

$$\delta q = \int_0^1 dx \Delta q \quad (8)$$

are often related to the hyperon beta decay constants F and D through the $SU(3)$ symmetry relations

$$\delta u + \delta \bar{u} - \delta d - \delta \bar{d} \equiv N_u - N_d = F + D = 1.2573 \quad (9)$$

$$\delta u + \delta \bar{u} + \delta d + \delta \bar{d} - 2(\delta s + \delta \bar{s}) \equiv N_u + N_d - 4N_s = 3F - D = 0.579. \quad (10)$$

Under such an assumption, the previous equations would strongly constrain the normalization of the quark densities. However, as we are not interested in forcing flavor symmetry, we leave aside that strong assumption and relax the symmetry relations introducing two parameters, ϵ_{Bj} and $\epsilon_{SU(3)}$ respectively. These parameters account quantitatively for eventual departures from flavor symmetry considerations, including also some uncertainties on the low- x behavior, and higher order corrections,

$$N_u - N_d = (F + D)(1 + \epsilon_{Bj}) \quad N_u + N_d - 4N_s = (3F - D)(1 + \epsilon_{SU(3)}), \quad (11)$$

and we take them as a measure of the degree of fulfillment of the Bjorken sum rule [20] and the $SU(3)$ symmetry.

Equations (11) allow to write the normalization of the three quark flavors in terms of N_s , ϵ_{Bj} , and $\epsilon_{SU(3)}$. Notice that no constraints have been imposed on the breaking parameters since we expect them to be fixed by data. The remaining parameters are constrained in such a way that positivity with respect to MRST02 parton distributions is fulfilled. These last parameterizations are used in order to compute the denominators of equations (1) and (3). Similar results are obtained with other modern sets of PDFs. Consistently with the choice for the unpolarized parton distributions, in order to compute α_s at LO and NLO we use the values of Λ_{QCD} obtained Ref.[12].

As anti-quark densities we take

$$x\Delta \bar{q} = N_{\bar{q}} \frac{x^{\alpha_{\bar{q}}} (1-x)^{\beta_{\bar{q}}}}{B(\alpha_{\bar{q}} + 1, \beta_{\bar{q}} + 1)} \quad \bar{q} = \bar{u}, \bar{d} \quad (12)$$

for \bar{u} and \bar{d} quarks, and we assume $\bar{s} = s$ since the possibility of discrimination in the s sector is beyond the precision of the data (as in the unpolarized case).

TABLE I: Inclusive and semi-inclusive data used in the fit.

Collaboration	Target	Final state	# points	Refs.
EMC	proton	inclusive	10	[23]
SMC	proton, deuteron	inclusive	12, 12	[24]
E-143	proton, deuteron	inclusive	82, 82	[25]
E-155	proton, deuteron	inclusive	24, 24	[26]
Hermes	proton,deuteron,helium	inclusive	9, 9, 9	[4]
E-142	helium	inclusive	8	[27]
E-154	helium	inclusive	17	[25]
Hall A	helium	inclusive	3	[29]
COMPASS	deuteron	inclusive	12	[5]
SMC	proton,deuteron	h^+, h^-	24, 24	[3]
Hermes	proton, deuteron, helium	$h^+, h^-, \pi^+, \pi^-, K^+, K^-, K^T$	36,63,18	[4]
Total			478	

Fragmentation functions are taken from either [11] or [10], respectively. We also use the flavor symmetry and flavor separation criteria proposed in [11], at the respective initial scales Q_i^2 .

$$\begin{aligned}
D_u^{\pi^+}(z, Q^2) &= D_d^{\pi^+}(z, Q^2) = D_{\bar{u}}^{\pi^-}(z, Q^2) = D_{\bar{d}}^{\pi^-}(z, Q^2) \\
D_u^{\pi^+}(z, Q_i^2) &= D_d^{\pi^+}(z, Q_i^2) = D_s^{\pi^+}(z, Q_i^2) = D_{\bar{s}}^{\pi^+}(z, Q_i^2) = D_s^{\pi^+}(z, Q_i^2) = (1-z) D_u^{\pi^+}(z, Q_i^2)
\end{aligned} \tag{13}$$

for the fragmentation into pions, which have shown to be in agreement with unpolarized SIDIS data [21], and

$$\begin{aligned}
D_u^{K^+}(z, Q^2) &= D_{\bar{u}}^{K^-}(z, Q^2) = (1-z) D_{\bar{s}}^{K^+}(z, Q^2) \\
D_d^{K^+}(z, Q_i^2) &= D_{\bar{d}}^{K^+}(z, Q_i^2) = D_s^{K^+}(z, Q_i^2) = D_{\bar{u}}^{K^+}(z, Q_i^2) = (1-z)^2 D_{\bar{s}}^{K^+}(z, Q_i^2)
\end{aligned} \tag{14}$$

for kaons.

The data sets analyzed include only points with $Q^2 > 1 \text{ GeV}^2$, listed in Table I, and totaling 137, 139, and 37 points, from proton, deuteron, and helium targets respectively, from pDIS plus 60, 87, and 18, from proton, deuteron, and helium targets respectively from pSIDIS. Notice that in the case of HERMES data, we have taken those coming from the most recent release, which include corrections for instrumental smearing and radiative effects

III. GLOBAL ANALYSES

As it is well known, there are various alternatives for defining the function to be minimized in the global fit [30, 31]. To begin with, we consider the most simple and commonly used in fits to polarized data, namely

$$\chi^2 = \sum_{i=1}^N \frac{(T_i - E_i)^2}{\sigma_i^2}, \tag{15}$$

where E_i is the measured value of a given observable, T_i is the corresponding theoretical estimate computed with a given set of parameters for the pPDFs, and σ_i is the error associated with the measurement, usually taken to be the addition of the reported statistical and systematic errors in quadrature. This definition ignores the correlations between data points from the same measurements, nevertheless it is widely used since in many cases the full correlation matrices are not available. In the cases where the correlation matrices between inclusive and semi-inclusive data are available, we have taken them into account by means of the appropriate definition for χ^2 [7].

In Table II, we summarize the results of the best NLO and LO global fits to all the data listed in Table I (478 data points). We present fits obtained using alternatively fragmentation functions from reference [11], labeled as KRE, and from reference [10], labeled as KKP. Since the fit involves 20 parameters, the number of degrees of freedom for these fits is 478-20=458. Consequently, the χ^2 values obtained are excellent for NLO fits and very good for LO. The better agreement between theory and experiment found at NLO, highlights the importance of the corresponding QCD corrections, for the present level of accuracy achieved by the data.

TABLE II: χ^2 values and first moments for distributions at $Q^2 = 10 \text{ GeV}^2$

set	χ^2	χ^2_{DIS}	χ^2_{SIDIS}	δu_v	δd_v	$\delta \bar{u}$	$\delta \bar{d}$	$\delta \bar{s}$	δg	$\delta \Sigma$
NLO	KRE 430.91	206.01	224.90	0.936	-0.344	-0.0487	-0.0545	-0.0508	0.680	0.284
	KKP 436.17	205.66	230.51	0.700	-0.255	0.0866	-0.107	-0.0454	0.574	0.311
LO	KRE 457.54	213.48	244.06	0.697	-0.248	-0.0136	-0.0432	-0.0415	0.121	0.252
	KKP 448.71	219.72	228.99	0.555	-0.188	0.0497	-0.0608	-0.0365	0.187	0.271

In NLO fits there seems to be better agreement when using KRE fragmentation functions, whereas at LO the situation is the opposite. The difference between the total χ^2 values between KRE and KKP NLO fits comes mainly from the contributions related to pSIDIS data, while those associated to inclusive data are almost the same, as one should expect in a fully consistent scenario. At variance with the NLO situation, in LO fits, the effect of pSIDIS data in the fit to inclusive data is strongly dependent on the set FFs used. This suggests a flaw in either the LO description of pSIDIS, the LO FFs used, or most likely in both of these ingredients. Notice also that KKP LO fit achieves a χ^2 to pSIDIS data close to those obtained at NLO, but the degree of agreement with inclusive data is several units poorer. KRE LO fit improves the agreement with inclusive data, but with a higher χ^2 to pSIDIS data.

Table II includes also the first moment of each flavor distribution at $Q^2 = 10 \text{ GeV}^2$, and that for the singlet distribution $\delta \Sigma$, as reference. Most noticeably, while the KRE NLO fit favors the idea of a SU(3) symmetric sea, KKP NLO finds \bar{u} polarized opposite to \bar{d} and to \bar{s} . Gluon and strange sea quark polarization are similar in both fits and the total polarization carried by quarks is found to be around 30%. At LO, KRE fits also prefers sea quarks polarized in the same direction although \bar{u} is much less polarized than \bar{d} and \bar{s} . KKP LO shows \bar{u} polarized opposite to \bar{d} and to \bar{s} as in NLO, and the total polarization is around 25%.

Notice that $\Delta u + \Delta \bar{u}$ and $\Delta d + \Delta \bar{d}$, could in principle be determined using inclusive data alone, with no dependence on a FFs. However, since pSIDIS data determine both $\Delta q + \Delta \bar{q}$ and $\Delta \bar{q}$, in the combined fit $\Delta q + \Delta \bar{q}$ ends with a small dependence on the FFs. The full set of parameters for the different sets can be found in Table A1, in the Appendix. A Fortran subroutine providing the scale dependent pPDFs can be obtained upon request from the authors.

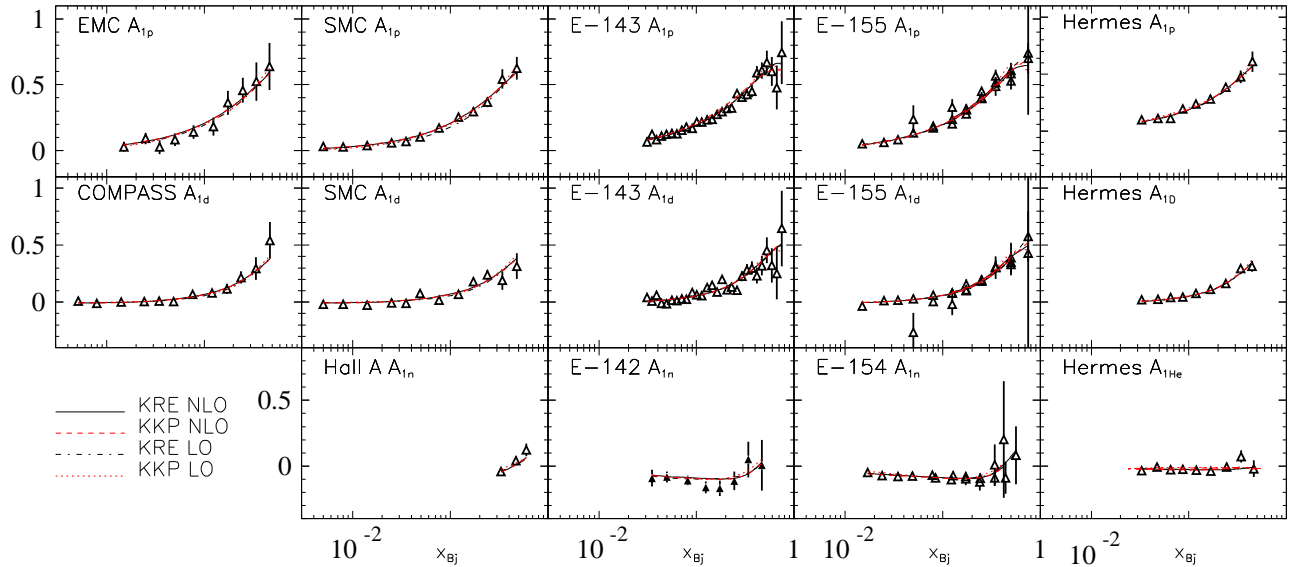


FIG. 1: Inclusive asymmetries computed with LO and NLO pPDFs against the corresponding data.

In Figures 1 and 2 we show the inclusive and semi-inclusive asymmetries computed with the different parameterizations both at LO and NLO accuracy, against the corresponding data sets. The differences between the various sets can

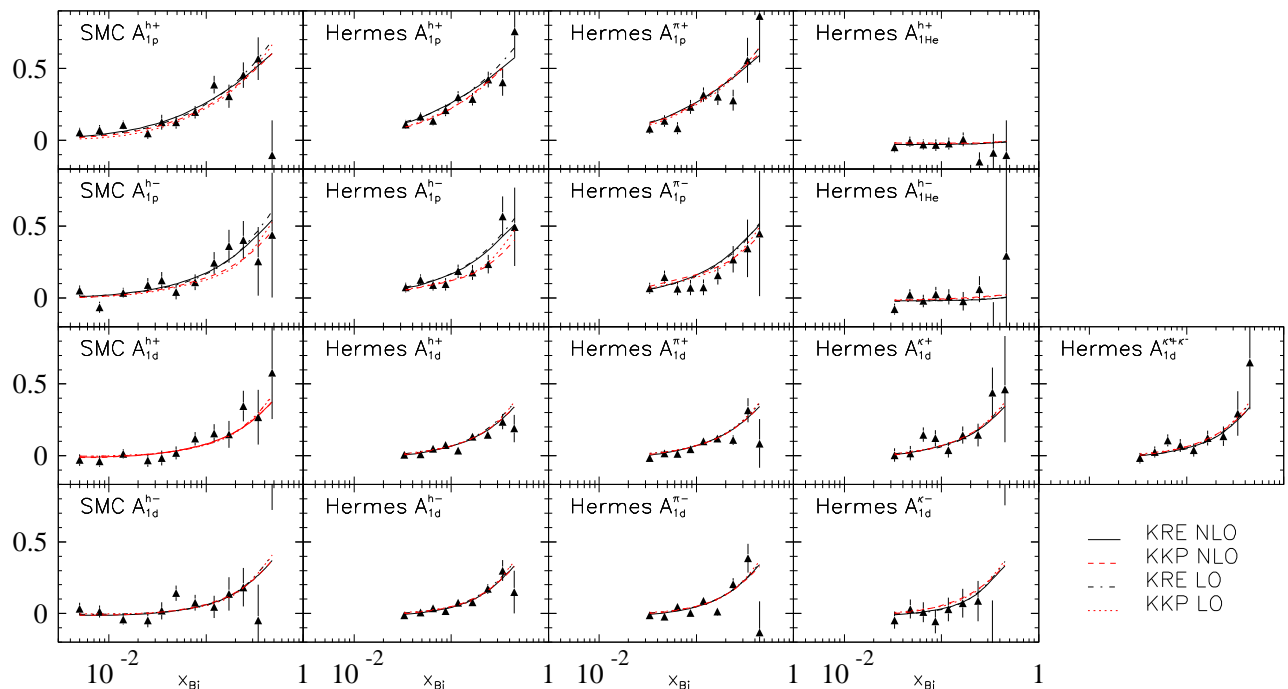


FIG. 2: Semi-inclusive asymmetries computed with LO and NLO pPDFs against the corresponding data.

hardly be noticed in the comparison to inclusive data in Figure 1, although are more significant when comparing to pSIDIS data, specially in the case of proton targets. This is due to the fact that the main difference between the sets are the light sea quark densities, which are probed by pSIDIS processes of proton targets. The pSIDIS asymmetries for deuterium targets are, of course, less sensitive to these differences since they average \bar{u} and \bar{d} contributions.

IV. UNCERTAINTIES

A crucial issue to be addressed before going any further in the interpretation of the results of the previous section is to estimate the uncertainties in the extraction of the individual pPDFs by means of the global fit, and also the uncertainty that will have any observable computed with them. This has been thoroughly studied in the context of unpolarized parton distributions, where the number and precision of the data available is much more significant, and the correct estimate of the uncertainties arising from PDF in predictions for observables related to new physics is mandatory [12, 30, 32].

The sources of uncertainty in PDFs are often classified into those associated with experimental errors on the data, and those associated with rather theoretical or phenomenological assumptions in the global fitting procedure, including: higher order QCD effects in the analyzed cross sections and their scale dependence, the particular choice of the parametric form of the distributions at the initial scale, nuclear target corrections, hadronization mechanisms and model assumptions such as $s = \bar{s}$. Clearly, while the first category is usually under control, the second one is particularly difficult to determine.

Many strategies have been implemented in order to assess the uncertainties in PDFs and their propagation to observables, specially those associated with experimental errors in the data. These include the Hessian approach, which assumes that the deviation in χ^2 for the global fit is quadratic in the deviations of the parameters specifying the input parton distributions, and then propagates linearly these uncertainties from PDFs to observables. Alternatively, the Lagrange multiplier method [30] probes the uncertainty in any observable or quantity of interest much more directly. This last method relates the range of variation of one or more physical observables dependent upon PDFs to the variation in the χ^2 used to judge the goodness of the fit to data. Specifically, it can be implemented minimizing

the function

$$\Phi(\lambda_i, a_j) = \chi^2(a_j) + \sum_i \lambda_i O_i(a_j) \quad (16)$$

with respect to the set of parameters a_j of the starting PDFs, for fixed values of the Lagrange multipliers λ_i . Each one of the parameters λ_i is related to an observable O_i , which is computed from the set of parameters a_j . For $\lambda_i = 0$ we get the best standard global fit, for which $\chi^2(a_j) = \chi_0^2$ and $O_i(a_j) = O_i^0$. Varying λ_i , and minimizing $\Phi(\lambda_i, a_j)$, the fit to data deteriorates increasing $\chi^2(a_j)$ from its minimum while $O_i(a_j)$ varies due to the different set of parameters a_j found. Performing a series of global fits for different values of λ_i , we get a profile of $\chi^2(a_j)$ for a range of values of the quantities O_i . In other words, this tell us how much the fit to data deteriorates if we force the PDFs to yield a prediction for an observable different to the one obtained with the best fit O_i^0 .

In order to illustrate the method and apply it to fits of polarized data, in Figure 3 we show the outcome of varying the χ^2 of the NLO fits to data against the first moment of the respective polarized parton densities δq at $Q^2 = 10 \text{ GeV}^2$, one at a time. This is, to minimize

$$\Phi(\lambda_q, a_j) = \chi^2(a_j) + \lambda_q \delta q(a_j) \quad q = u, \bar{u}, d, \bar{d}, s, g. \quad (17)$$

Of course, beyond LO, these first moments are not, strictly speaking, physical observables, however are perfectly well defined quantities once the factorization prescription is fixed. The solid lines in Figure 3 correspond to the KRE NLO fit (using as input for fragmentation functions those of reference [11]) while the dashed lines correspond KKP NLO (using [10]).

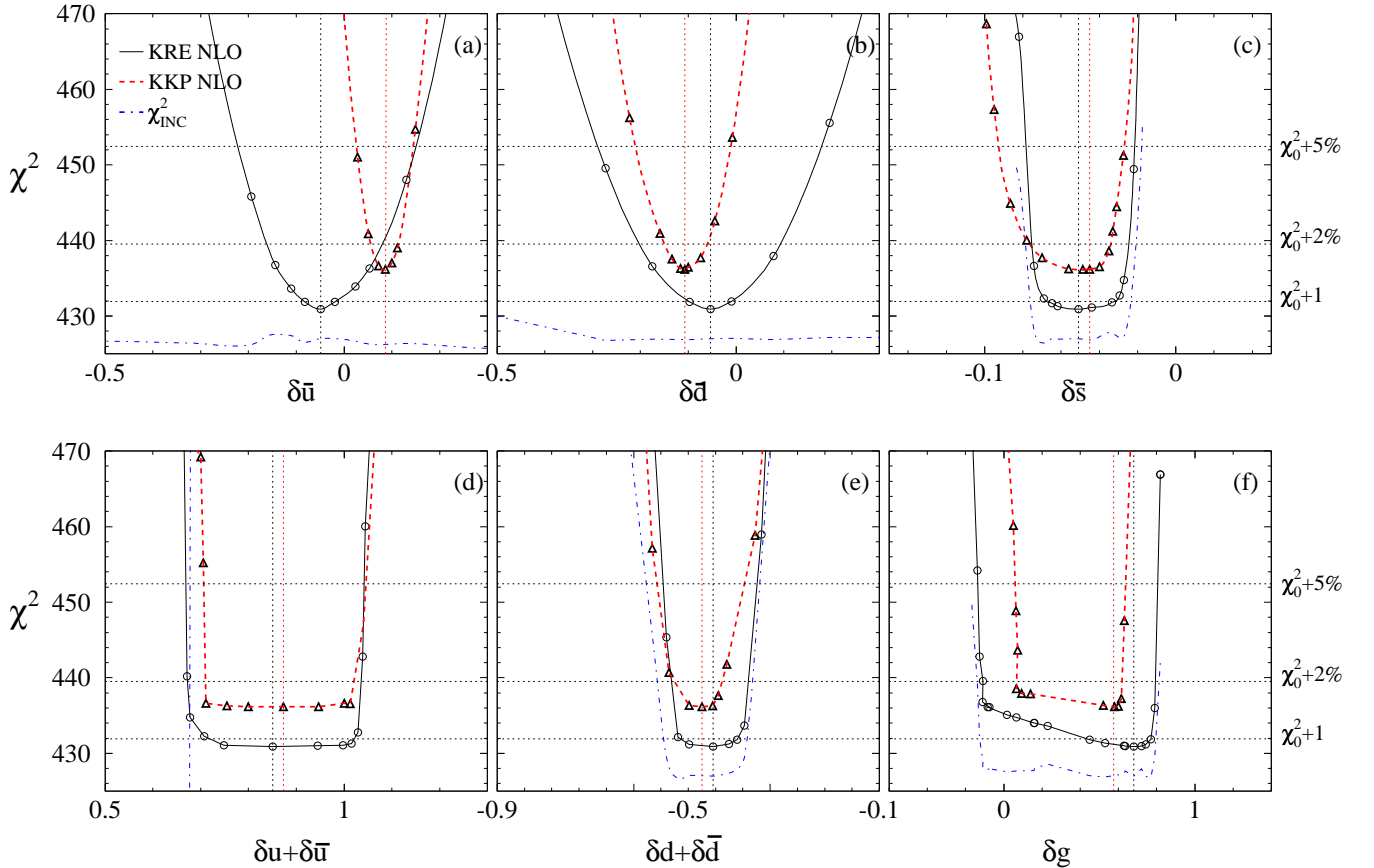


FIG. 3: χ^2 profiles for NLO fits obtained using Lagrange multipliers at $Q^2 = 10 \text{ GeV}^2$.

In an *ideal* situation, i.e. to have reliable estimates of every source of uncertainty, of correlated experimental and theoretical errors, and a quadratic dependence of χ^2 in the parameters of the fit, the profile of χ^2 would be just a

parabola and the 1σ uncertainty in any observable would correspond to $\Delta\chi^2 = 1$. In order to account for unexpected sources of uncertainty, in modern unpolarized global analysis it is customary to consider instead of $\Delta\chi^2 = 1$ between a 2% and a 5% variation in χ^2 as conservative estimates of the range of uncertainty.

As expected in the *ideal* framework, the dependence of χ^2 on the first moments of \bar{u} and \bar{d} resemble a parabola (Figures 3a and 3b). The KKP curves are shifted upward almost six units relative to those from KRE, due to the difference in χ^2 of their respective best fits. Although this means that the overall goodness of KKP fit is poorer than KRE, $\delta\bar{d}$ and $\delta\bar{u}$ seem to be more tightly constrained. The estimates for $\delta\bar{d}$ computed with the respective best fits are close and within the $\Delta\chi^2 = 1$ range, suggesting something close to the *ideal* situation. However for $\delta\bar{u}$, they only overlap allowing a variation in $\Delta\chi^2$ of the order of a 2%. This is a very good example of how the $\Delta\chi^2 = 1$ does not seem to apply due to an unaccounted source of uncertainty: the differences between the available sets of fragmentation functions.

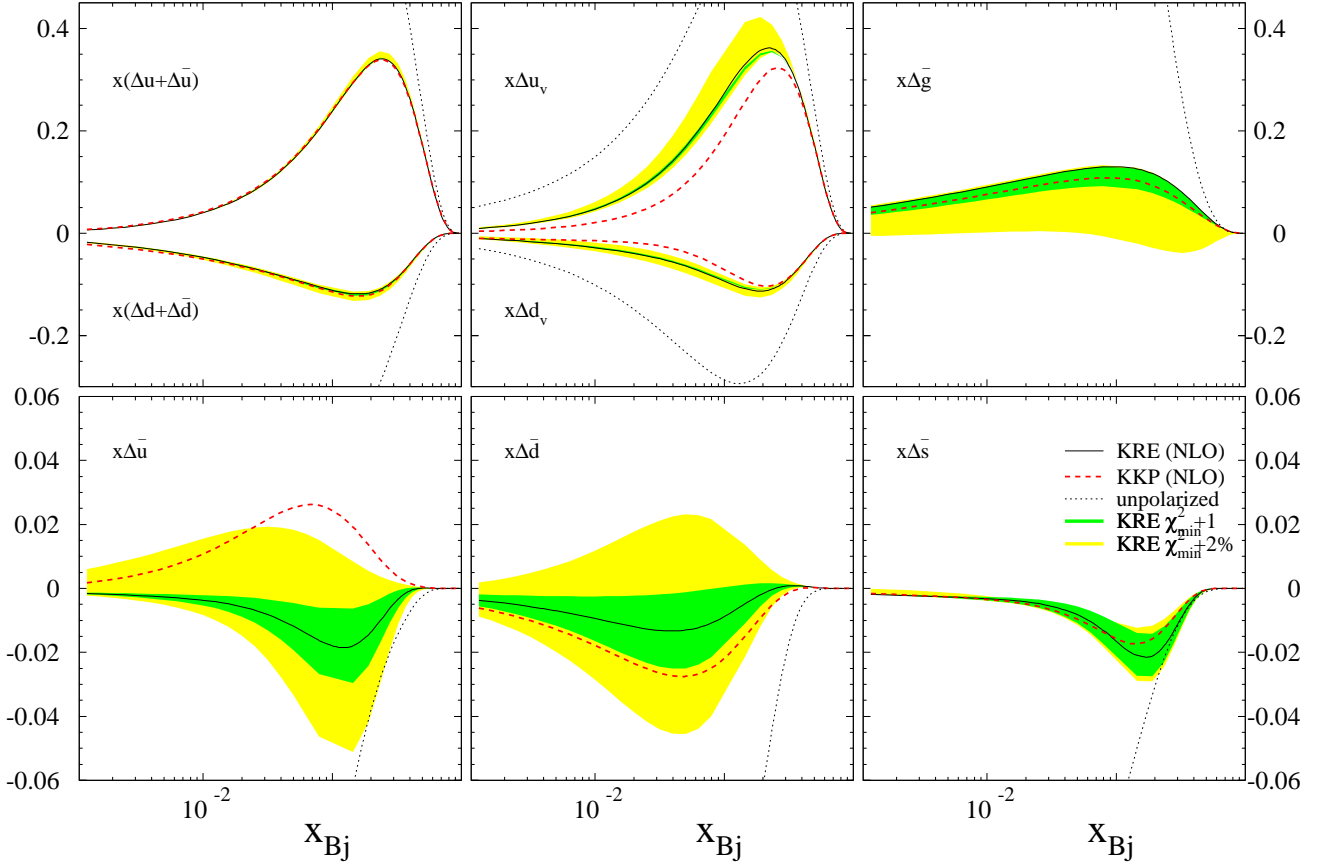


FIG. 4: Parton densities at $Q^2 = 10 \text{ GeV}^2$, and the uncertainty bands corresponding to $\Delta\chi^2 = 1$ and $\Delta\chi^2 = 2\%$

An interesting thing to notice is that almost all the variation in χ^2 comes from the comparison to pSIDIS data. The partial χ^2 value computed only with inclusive data, χ^2_{pDIS} , is almost flat reflecting the fact the pDIS data are not sensitive to \bar{u} and \bar{d} distributions. In Figure 3, we plot χ^2_{pDIS} with an offset of 206 units as a dashed-dotted line.

The situation however changes dramatically when considering $\delta\bar{s}$ or δg as shown in Figures 3c and 3f, respectively. In the case of the variation with respect to $\delta\bar{s}$, the profile of χ^2 is not at all quadratic, and the distribution is much more tightly constrained (notice that the scale used for $\delta\bar{s}$ is almost four times smaller than the one used for light sea quarks moments). The χ^2_{pDIS} corresponding to inclusive data is more or less indifferent within an interval around the best fit value and increases rapidly on the boundaries. This steep increase is related to a positivity constraints on Δs and Δg . pSIDIS data have a similar effect but also helps to define a minimum within the interval. The preferred values for δs obtained from both NLO fits are very close, and in the case of KRE fits, it is also very close to those obtained for $\delta\bar{u}$ and $\delta\bar{d}$ suggesting SU(3) symmetry.

For the total u and d polarization $\delta u + \delta \bar{u}$ and $\delta d + \delta \bar{d}$, the absolute uncertainties are large as shown in Figures 3d and 3e respectively, however their values relative to the best fit results are significantly smaller than for sea quarks. For δg , again χ^2_{pDIS} just defines an interval, as it has been pointed out in previous analyses [7, 8], bounded by its own positivity constraint in the upper end, and by those of the sea quarks densities, which grow in the lower end. Between both ends, there is either some redundancy of parameters or a need of more sensitive data. Again, semi-inclusive data help to define a minimum, and it is very close for both fits. Within the $\Delta\chi^2 = 2\%$ uncertainty, the gluon polarization estimate is in agreement with a recent analysis of high p_T hadron production [33]

Clearly, in the case of $\delta \bar{s}$ or δg , the simple minded use of the Hessian approach does not apply. In the case of the light sea, the sensitivity to a smaller and internally consistent data set, presumably put us closer to the ideal situation.

In order to see the effect of the variation in χ^2 on the parton distributions themselves, in Figure 4, we show KRE best fit densities together with the uncertainty bands corresponding to $\Delta\chi^2 = 1$ (darker band) and $\Delta\chi^2 = 2\%$ (light shaded band). As expected, the relative uncertainties in the total quark densities and those strange quarks are rather small. For gluon densities the $\Delta\chi^2 = 1$ band is also small, but the most conservative $\Delta\chi^2 = 2\%$ estimate is much more significant. For light sea quarks the $\Delta\chi^2 = 1$ bands are moderate but the $\Delta\chi^2 = 2\%$ are much more larger.

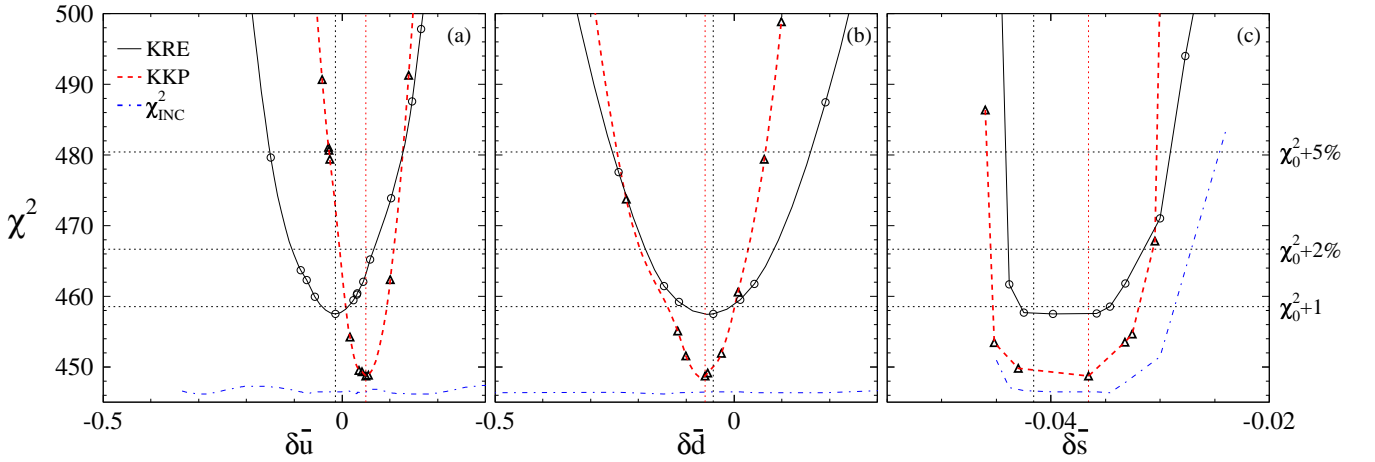


FIG. 5: χ^2 profiles for LO fits obtained using Lagrange multipliers at $Q^2 = 10 \text{ GeV}^2$.

The profiles for χ^2 obtained with LO fits show similar features to those obtained at NLO. In Figure 5 we show the LO profiles for sea quark densities. Notice that before reaching any conclusion about the uncertainties obtained in LO and their comparison with those found in NLO a few remarks are in order. In the first place, the rather large difference between the LO and NLO χ^2 values in fits to the same sets of data implies that the uncertainties due to use of one or the other approximation, and their related ingredients, are not properly accounted for. Any mean to include these uncertainties would certainly reduce the constraining power of the LO fit and thus increase the uncertainties on the pPDFs. Unfortunately there is no evident way to do this and also to relate the criteria used to go from profiles to uncertainties in NLO and LO. The second point is related to the fact that beyond the LO PDFs are factorization scheme dependent and thus the relation between the LO and NLO PDFs and their uncertainties is even less direct.

The Lagrange multiplier method allows also to analyze the interplay and consistency between inclusive and semi-inclusive data [9] we mentioned in the previous section. The idea is to apply a Lagrange multiplier to the pSIDIS contribution to the function to be minimized,

$$\Phi(\lambda, a_j) = \chi^2_{pDIS}(a_j) + \lambda \chi^2_{pSIDIS}(a_j) \quad (18)$$

and perform global fits for different values of λ . For λ values lower than unity, the weight of pSIDIS data in the fit is artificially reduced and the fit becomes increasingly dominated by pDIS data as $\lambda \rightarrow 0$. The partial contribution of pDIS data to χ^2 , χ^2_{pDIS} , decreases up to a saturation point given by the best fit to pDIS data only, while that of pSIDIS data, χ^2_{pSIDIS} , increases. Using λ values larger than unity, the fit becomes dominated by pSIDIS data, until it saturates at the best fit to pSIDIS data alone.

In Figure 6 we show the results for χ^2_{pDIS} vs. χ^2_{pSIDIS} in fits with a wide range of values of λ in Eq. 18 for KRE

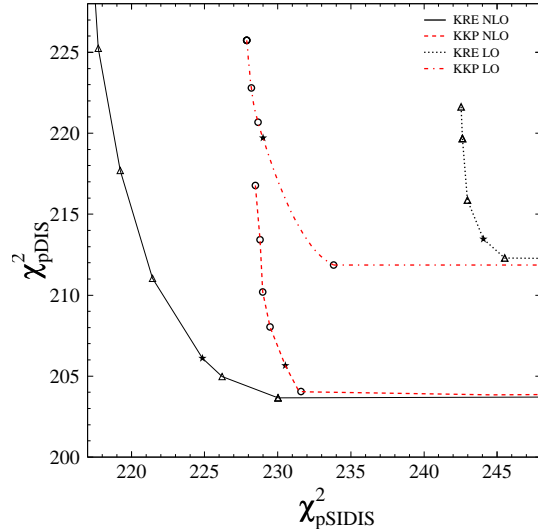


FIG. 6: χ_{pDIS}^2 vs. χ_{pSIDIS}^2 for KRE and KKP NLO and LO fits

NLO (solid line), KKP NLO (dashed line), KRE LO (dotted line) and KKP LO fits (dotted-dashed line), respectively. The standard best fit in each curve ($\lambda = 1$) is denoted by a star.

In both NLO curves, the χ_{pDIS}^2 values obtained in the best standard fits, are very close to the common saturation value, corresponding to a fit without pSIDIS data. This suggests a high degree of compatibility between both data sets in a NLO framework, since the inclusion of pSIDIS data does not worsens significantly the agreement with pDIS data. The increase in the relative weight of pSIDIS data reduces χ_{pSIDIS}^2 only in a couple of units in the case KKP fits, what indicates that the fit is strongly constrained and that the best fit result for χ_{pSIDIS}^2 is close to its saturation value. However, χ_{pSIDIS}^2 in the best KRE NLO is several units smaller although with a χ_{pDIS}^2 similar to that of KKP. The saturation value obtained in this case is also much smaller. These last features mean that KRE FFs allow a much better and flexible fit to pSIDIS data.

For LO the situation is quite different: the common saturation value for χ_{pDIS}^2 is several units larger than the found at NLO, what means that even neglecting pSIDIS data the fits obtained at LO are poorer than those of NLO accuracy. The best KRE LO fit value for χ_{pDIS}^2 is close to the saturation value, but at the expense of a rather large χ_{pSIDIS}^2 value. In the case of KKP LO fit, χ_{pSIDIS}^2 improves significantly but the departure of χ_{pDIS}^2 from its saturation value is very large.

V. FUTURE PROSPECTS

One of the measurements most eagerly awaited by the spin physics community is that of single inclusive large p_T pion production in longitudinally polarized proton-proton collisions, which is right now being run at BNL RHIC [34]. The spin dependent asymmetry associated to this kind of process, $A_{LL}^{\pi^0}$ is defined, as usual, in terms of the ratio between the polarized and the unpolarized cross sections,

$$A_{LL}^{\pi^0} = \frac{d\Delta\sigma^{pp \rightarrow \pi^0 X}}{d\sigma^{pp \rightarrow \pi^0 X}} \quad (19)$$

which is strongly dependent on the gluon polarization. Indeed, in this observable polarized gluons show up in the cross section in the dominant terms. The NLO QCD corrections to this observable have been computed recently [35, 36] finding both large QCD corrections, which make unavoidable the use of the NLO approach, and also a very significant dependence on Δg , features that in principle would help to constrain the amount of gluon polarization in much more stringent way than in DIS experiments.

The data obtained up to now by the PHENIX Collaboration suggest a very small asymmetry, consistent with pPDFs sets with a moderate gluon polarization. In the following we apply the Lagrange multiplier method in order

to explore the range of variation of the estimates for this asymmetry associated to the uncertainty in the present extraction of pPDFs.

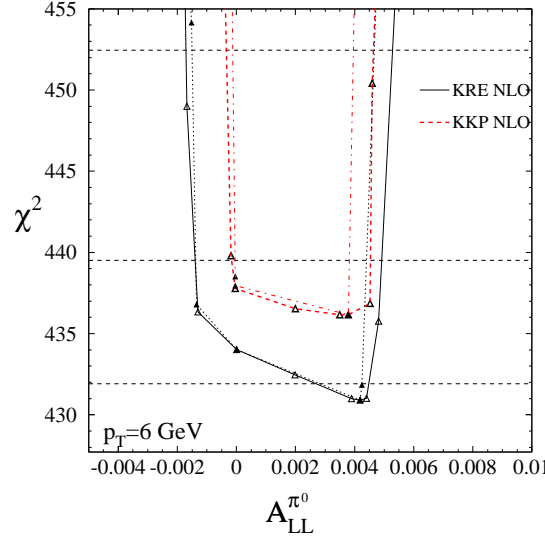


FIG. 7: Profile of the global χ^2 to data against $A_{LL}^{\pi^0}$ at $p_T = 6$ GeV

In Figure 7 we show the range of variation of $A_{LL}^{\pi^0}$ at an intermediate value for $p_T = 6$ GeV obtained with different sets of pPDFs against the variation of the χ^2 to pDIS and pSIDIS data for these distributions. The profile of χ^2 defines a well defined range of values for $A_{LL}^{\pi^0}$ allowed by present pPDFs. The solid line represents the profile of χ^2 obtained using KRE FFs, both in the global fit to data and in the computation of the asymmetry. The dashed line represents the same but for KKP FFs. The minima corresponding to both profiles are very close suggesting a cancellation of the associated uncertainty. Notice that both the extraction of the pPDFs, and also the estimate of $A_{LL}^{\pi^0}$ with a given set, rely on a set of FFs. The double dependence of the observable on the set of FFs used may had, in principle, even potentiated the disagreement.

Notice that when the fitting procedure explores alternative sets of pPDFs in order to minimize or maximize the value of $A_{LL}^{\pi^0}$, not only the gluon distributions varies, but all the distributions. Since the observable is strongly dependent on the gluon polarization, there is a very tight correlation between $A_{LL}^{\pi^0}$ and δg , reflected by the fact that almost the same sets that maximize/minimize the asymmetry, maximize/minimize δg , however the role of sea quark polarization is non negligible.

In Figure 7 we have included also the profiles obtained using δg instead of $A_{LL}^{\pi^0}$ in minimization as a dotted line in the case of KRE and a dashed dotted line for KKP. Clearly, the sea quark polarization can conspire in order to yield a larger/smaller asymmetry than the one obtained with maximum/minimum gluon fit at a given χ^2 , effect which is much more apparent at larger values of $A_{LL}^{\pi^0}$. This feature will have to be taken into account in the future for a very precise measurement of the gluon polarization.

Unfortunately, the data collected so far in the first two runs of the PHENIX detector at RHIC have estimated errors much larger than the uncertainties in the values $A_{LL}^{\pi^0}$ coming from the fits, however this situation is going to change dramatically in the near future. In Figure 8 we plot $A_{LL}^{\pi^0}$ as a function of p_T using the best NLO fits coming from KRE and KKP FFs (solid lines and dashes, respectively) and also with KRE variants designed to enhance/reduce $A_{LL}^{\pi^0}$ with $\Delta\chi^2 = 2\%$ (dotted-dashed lines). We have also included the expected uncertainties for the next two runs centered at KRE best fit estimate [37]. Clearly, the future measurement of the asymmetry would certainly be able to constrain even further the gluon and therefore reduce the uncertainties in pPDFs.

Another source of complementary information to further constrain the extraction of pPDFs and also FFs is the experimental program of the E04-113 experiment at JLAB, which propose to measure pion and kaon pSIDIS asymmetries for proton and deuteron targets [6]. In Figure 9a we show the profile of χ^2 of the global fits using KRE (solid line) and KKP (dashes) FFs against the π^- pSIDIS asymmetry on proton targets at one of the kinematic configurations of E04-113 ($x_B j = 0.203$, $Q^2 = 2.3 \text{ GeV}^2 < z < 0.5$). The expected uncertainty for the measurement of this asymmetry shown in the bottom of the figure, is significantly smaller than those of the previous measurements, and also smaller

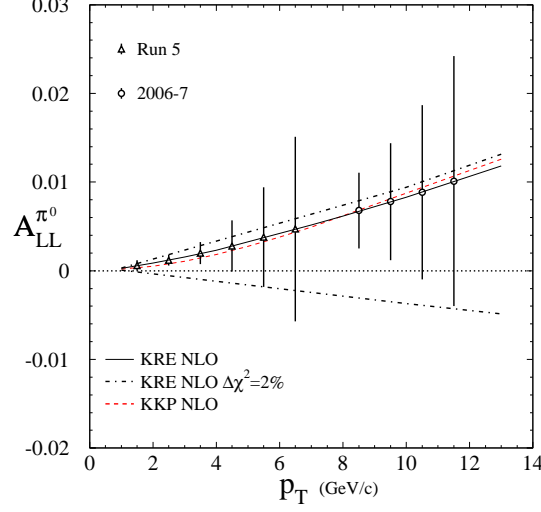


FIG. 8: $A_{LL}^{\pi^0}$ vs. p_T computed with different pPDF sets and the estimated errors expected by PHENIX at RHIC.

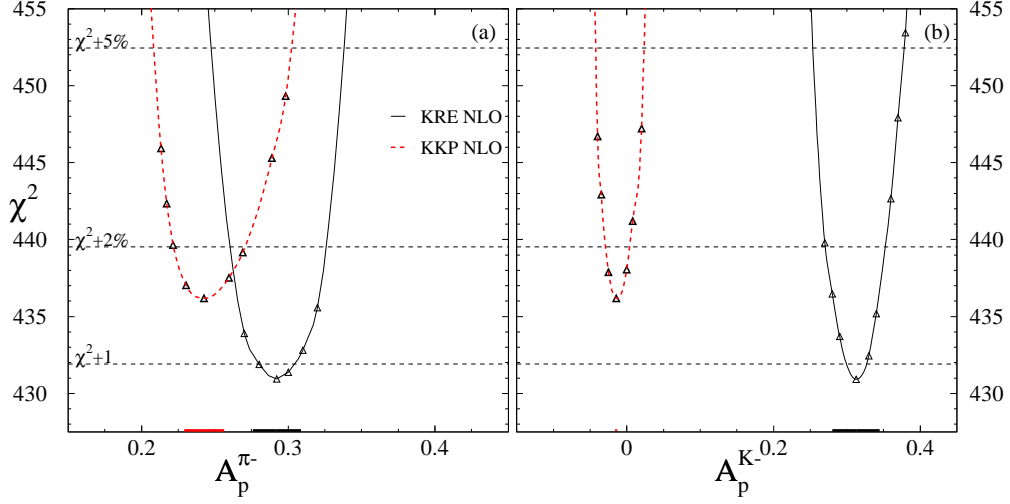


FIG. 9: Profile of the global χ^2 to data against $A_p^{\pi^-}$ and $A_p^{K^-}$ proposed to be measured by E04-113 at JLAB.

than the present uncertainty coming from the fit. In Figure 9b we show the same as in the previous figure but for negative kaons. This asymmetry has not been measured yet and the difference between the predictions coming from KRE (solid line) and KKP (dashed) sets is much larger than the expected uncertainties. The measurement of this last observable together with the combined effect of data for different targets (proton and deuteron) and final state hadrons (positive and negative pions and kaons) will certainly constrain the fit even further, specifically the sea quark densities, and at the same time provide a more stringent test on the quark flavor separation for the FFs used in the analysis.

VI. CONCLUSIONS

The availability of an important set of new data on polarized processes together with the appropriate theoretical tools required to interpret them, obtained and developed in the last few years, have led the extraction of pPDFs in the proton to mature and to become an important source of information which will still keep growing in the near future.

In this paper, we have assessed the feasibility of obtaining pPDFs, with special emphasis on the sea quark densities, from a combined NLO QCD analysis of pDIS and pSIDIS data. We have estimated the uncertainties associated to the extraction of each parton density, finding a well constrained scenario. pSIDIS data is not only consistent with pDIS, but improves the constraining power of the fit for all the distributions, being crucial for the light sea quarks.

Different choices for the FFs used in the analysis of pSIDIS data lead to differences in the light sea quark pPDFs, although these differences are within a conservative uncertainty estimate for them. While KRE FFs favor a SU(3) flavor symmetric sea, KKP FFs suggest an SU(3) broken one, however the former led to fits of much better quality.

The first moment of the gluon distribution at a 10 GeV² is found to be close to 0.6, constrained to be smaller than 0.8 and larger than -0.05 within a conservative $\Delta\chi^2 = 2\%$ range. The upper constraint coming from the requirement of positivity of the gluon density and the lower one due to the QCD evolution which forces sea quark densities to saturate their own positivity constraints.

The overall picture found for the quark densities at a 10 GeV² is one in which, within uncertainties, up quarks are almost 100% polarized parallel to the proton, down quarks anti-parallel in a similar proportion, and sea quarks have a small flavor symmetric negative polarization.

Two programmed experiments, the one based on the PHENIX detector already running at RHIC, and the E04-113 experiment at JLab will be able to reduce dramatically the uncertainty in both the gluon and the light sea quark densities respectively, the latter providing also an even more stringent test on fragmentation functions.

VII. ACKNOWLEDGEMENTS

We warmly acknowledge W. Vogelsang, S. Kretzer, C. A. García Canal and Xiaodong Jiang for comments and suggestions, Y. Fukao for providing PHENIX error estimates.

-
- [1] A. D. Martin, R. G. Roberts, W. J. Stirling and R. S. Thorne, arXiv:hep-ph/0411040.
 - [2] J. Pumplin, D. R. Stump, J. Huston, H. L. Lai, P. Nadolsky and W. K. Tung, JHEP **0207** (2002) 012 [arXiv:hep-ph/0201195].
 - [3] B. Adeva et al., SMC Collab., Phys. Lett. **B369**, 93 (1996), ibid. **420** 180 (1998).
 - [4] HERMES Collab., A. Airapetian, et al. hep-ex/0407032; K. Ackerstaff et al., Phys. Lett. **B464**, 123 (1999).
 - [5] A. Bressan, for the COMPASS Collaboration, hep-ex/0501040.
 - [6] X. Jiang et al. Jefferson Lab experiment E04-113: Semi-Inclusive Spin Asymmetries on the Nucleon Experiment (hep-ex/0412010).
 - [7] D. de Florian, O. A. Sampayo, R. Sassot, Phys. Rev. D **57** 5803 (1998).
 - [8] D. de Florian, R. Sassot, Phys. Rev. D **62** 094025 (2000).
 - [9] G. A. Navarro and R. Sassot, Eur. Phys. J. C **28**, 321 (2003) [arXiv:hep-ph/0302053].
 - [10] B. A. Kniehl, G. Kramer and B. Potter, Nucl. Phys. B582 (2000) 514 [arXiv:hep-ph/0010289].
 - [11] S. Kretzer, Phys. Rev. D62 (2000) 054001. [arXiv:hep-ph/0003177].
 - [12] A. D. Martin, R. G. Roberts, W. J. Stirling and R. S. Thorne, Eur. Phys. J. C28 (2003) 455 [arXiv:hep-ph/02112080].
 - [13] D. de Florian, C. A. Garcia Canal and R. Sassot, Nucl. Phys. B **470**, 195 (1996) [arXiv:hep-ph/9510262].
 - [14] B. Lampe and E. Reya, Phys. Rep. 332, 1 (2000);
E. Leader et al., Phys. Rep. 261, 1 (1995).
 - [15] R. Mertig, W. L. van Neerven, Z.Phys.**C70**, 637,(1996); W. Vogelsang, Phys.Rev.**D54**,20023, (1996).
 - [16] M. Glück, E. Reya and W. Vogelsang, Phys.Rev.**D53**,6100 (1996).
 - [17] E. Leader, A. V. Sidorov and D. B. Stamenov, arXiv:hep-ph/0503140.
 - [18] D. de Florian, C.A. Garcia Canal, and R. Sassot, Nucl. Phys. **B470**, 195 (1996).
 - [19] M. Stratmann, W. Vogelsang, Phys. Rev. D **64**, 114007 (2001).
 - [20] J.D. Bjorken, Phys. Rev. **148**, 1467 (1966).
 - [21] S. Kretzer, E. Leader, E. Christova, Eur. Phys. J. **C22**, 269 (2001) .
 - [22] J. Ellis and R.L. Jaffe, Phys. Rev. D **9**, 1444 (1974)..
 - [23] EMC Collaboration, J. Ashman et al., Nucl. Phys. **B328**, 1 (1989).
 - [24] SMC Collaboration, B. Adeva et al., Phys. Rev. **D58**, 112001 (1998).

- [25] E143 Collaboration, K. Abe et al, Phys. Rev. D **58**, 112003 (1998).
- [26] E155 Collaboration, P. L. Anthony, et al., Phys. Lett. **B463**, 339 (1999); G. S. Mitchell, Ph.D. Thesis University of Wisconsin-Madison, SLAC-Report-540 (1999)
- [27] E142 Collaboration, P. L. Anthony, et al., Phys. Rev. D **54**, 6620 (1996).
- [28] E154 Collaboration, K. Abe et al., Phys. Rev. Lett. **79**, 26 (1997); Phys. Lett. **B405**, 180 (1997).
- [29] HALL A Collaboration X. Zheng, et al., nucl-ex/0405006
- [30] J. Pumplin, D. R. Stump and W. K. Tung, Phys. Rev. D **65**, 014011 (2002) [arXiv:hep-ph/0008191];
D. Stump *et al.*, Phys. Rev. D **65**, 014012 (2002) [arXiv:hep-ph/0101051].
- [31] R. S. Thorne, arXiv:hep-ph/0211113.
- [32] M. Botje, Eur. Phys. J. **C14** (2000) 285.
- [33] J. R. Ellis and M. Karliner, arXiv:hep-ph/0501115.
- [34] S. S. Adler *et al.* [PHENIX Collaboration], Phys. Rev. Lett. **93** (2004) 202002 [arXiv:hep-ex/0404027].
- [35] D. de Florian, Phys. Rev. D **67**, 054004 (2003) [arXiv:hep-ph/0210442].
- [36] B. Jäger, A. Schafer, M. Stratmann and W. Vogelsang, Phys. Rev. D **67**, 054005 (2003) [arXiv:hep-ph/0211007].
- [37] Y. Fukao [PHENIX Collaboration], arXiv:hep-ex/0501049.

Appendix: Parameters of the fits

We present here the parameters of the best fits found in our analyses, both at LO and NLO.

Parameter	KRE NLO	KKP NLO	KRE LO	KKP LO
ϵ_{BJ}	-0.0067	0.0280	-0.1994	-0.2413
$\epsilon_{SU(3)}$	-0.0122	-0.0795	-0.15	-0.1
α_u	1.2024	1.0908	0.8376	1.1325
β_u	3.4517	3.2909	3.5832	4.3992
γ_u	7.4178	9.2128	10.270	13.287
δ_u	1.0722	0.9956	1.4483	2.2157
α_d	0.6717	0.4913	0.6431	0.8770
β_d	4.7090	4.3816	4.9575	5.4356
γ_d	14.999	19.999	14.999	14.999
δ_d	1.5666	1.3891	1.8938	2.4361
N_s	-0.0441	-0.0398	-0.0367	-0.0382
α_s	3.500	2.5000	2.1045	3.4466
$\beta_s = \beta_{\bar{u}} = \beta_{\bar{d}}$	11.741	9.7131	9.8861	14.997
$N_{\bar{u}}$	-0.0444	0.0799	-0.0122	0.0453
$\alpha_{\bar{u}}$	2.500	1.1332	2.5828	1.1892
$N_{\bar{d}}$	-0.0454	-0.0971	-0.0408	-0.0557
$\alpha_{\bar{d}}$	0.9970	0.8979	0.73443	1.0639
N_g	0.1273	0.0781	0.1965	0.082
α_g	2.398	2.2901	0.0390	1.320
β_g	2.1398	1.5698	2.4051	4.485
χ^2_{Total}	430.91	436.17	457.52	448.71
χ^2_{DIS}	206.01	205.66	213.48	228.99
χ^2_{SIDIS}	224.90	230.51	219.72	228.99

Table A1: Coefficients for NLO and LO best fits